Advances in Science and Technology Research Journal

Advances in Science and Technology Research Journal, 2027, 21(1), 411–426
https://doi.org/10.12913/22998624/235987
ISSN 2299-8624, License CC-BY 4.0

Received: 2026.08.06
Accepted: 2026.11.15
Published: 2026.12.01

Numerical design and evaluation of locally resonant elements for vibration attenuation in an automobile door

Nguyen Thanh Cong[1], Le Duc Hieu[2], Nguyen Trung Kien[2], Nguyen Phi Truong[2*]

[1] Faculty of Mechanical Engineering, University of Transport and Communications, Hanoi, Vietnam
[2] Faculty of Transportation Engineering, School of Mechanical and Automotive Engineering, Hanoi University of Industry, Hanoi, Vietnam
* Corresponding author's e-mail: truongnp@haui.edu.vn

ABSTRACT

This study examines the impact of resonant elements on the vibration absorption capability of car door constructions. Utilizing vibration theory, this study ascertains the open and closed intervals of the absorption spectrum (bandgap) to enhance vibration attenuation efficacy. Simulation results indicate that resonant elements can provide a broad bandgap and effectively attenuate vibrations at targeted frequencies of 25 Hz, 60 Hz, and 150 Hz. The numerical evaluation demonstrates that installing these resonators reduces maximum displacement by ratios of 8.86, 4.04, and 5.27 for 25, 60, and 150 Hz, respectively. The total added mass of the resonators is approximately 1.21 kg. The use of resonant elements into doors markedly improves vibration absorption capabilities while maintaining the structural integrity due to their small dimensions. The study validates that the implementation of resonant elements constitutes an efficient and viable numerical method for mitigating vibrations in door structures, with potential for extensive application in engineering systems necessitating vibration control without modification of the original structure

Keywords: phononic band gap, passive vibration control, finite-element analysis, COMSOL Multiphysics, automotive NVH, metal additive manufacturing.

INTRODUCTION

Undesired vibrations in vehicles originate from various sources, often linked to operational conditions and environmental factors. The causes include uneven road surfaces, imbalanced weight distribution, and the operation of mechanical components. These variables increase vibration levels, thereby affecting the stability, durability, and comfort of the driver. The quality of the pavement is the most significant element among them. Defects such as potholes, bumps, or uneven surfaces can produce considerable excitation forces on the suspension system, leading to oscillation of the vehicle body. Multiple studies demonstrate that pavement quality and internal engine oscillations substantially affect riding comfort and operational safety [1–3]. A well-maintained road surface diminishes vibration, but a degraded road surface increases the likelihood of instability and causes discomfort for passengers.

Furthermore, automotive engines provide a significant source of vibration, especially during acceleration or deceleration. Vibrations generated by rotational forces and drivetrain imbalances can transmit to the vehicle chassis and passenger compartment, intensifying the perception of shaking. Aerodynamic forces acting on the vehicle body at elevated speeds can also generate oscillations, reducing the vehicle's control and stability [4,5]. Additionally, changes in load, such as passenger numbers or cargo weight, affect the center of gravity, leading to variations in oscillation characteristics. Asymmetrical load distribution amplifies the risk of substantial vibrations or instability [6,7].

Thus, exploring and applying techniques to reduce or eliminate oscillations has become a vital priority for enhancing safety and driving pleasure. In recent years, many advanced technical solutions have been developed. An efficient technique is electronically controlled suspension, which allows for the modulation of damping stiffness based on road conditions and driving behavior, hence significantly improving ride comfort and stability [8]. Moreover, optimizing the vehicle body's aerodynamics reduces drag, enhances fuel efficiency, and minimizes vibrations at high speeds. The use of vibration-dampening materials, such as rubber, composite substances, or smart materials, aims to minimize the transmission of vibrations from the road surface to the vehicle chassis, consequently improving the tranquility and comfort of the cabin environment [9].

A plethora of research studies have been conducted globally and in Vietnam to investigate the origins, transmission processes, and effects of vehicle vibrations [10, 11]. Various researchers have developed both linear and non-linear vehicle oscillation simulation models and traffic oscillation propagation models, thereby improving the comprehension of oscillation behavior in practical situations [12–14]. Simultaneously, extensive empirical studies on vehicle transmission and suspension vibrations have been documented in the domestic Vietnamese context [15–17]. Simultaneous research efforts are focusing on advanced vibration-dampening materials. Laminate panels, metabsorber materials, and elastic composites have proven effective in mitigating vibrations in the low and medium frequency ranges [18–21]. The amalgamation of optimal structural design and intelligent materials that absorb vibrational energy is promoting more efficient progress in vibration control. Recent studies have focused on developing elastic resonant components capable of dissipating energy and reducing structural vibrations [22–26].

Despite significant developments, most current treatments primarily focus on the suspension or chassis framework, while other components, such as car doors, remain markedly affected by residual vibrations. Car doors, due to their thin, sheet-like construction, demonstrate increased susceptibility to environmental and mechanical vibrations, leading to the transfer of these vibrations into the passenger compartment. Conventional passive material options, including rubber layers or composite laminates, are significantly influenced by frequency, and a considerable reduction at low frequencies generally requires increased thickness and mass, which is at odds with the principles of lightweight automotive construction.

Recently, locally resonant metamaterials and phononic structures have emerged as feasible alternatives for passive vibration control. Compact resonant elements can provide locally resonant band gaps, enabling efficient vibration attenuation in low- and medium-frequency bands without a considerable mass increase. While several cited studies already address locally resonant metamaterials in automotive structures—including applications to vehicle shock towers and tyre noise—their specific application to thin-walled automobile doors facing complex, multi-frequency excitations remains insufficiently explored. The specific novelty of this study lies in the numerical development of a multi-frequency resonator configuration targeting 25, 60, and 150 Hz simultaneously, coupled with a positioning strategy that strategically places sets of resonators only at localized high-displacement regions rather than utilizing uniform structural coverage.

Therefore, the primary objective of this research is to numerically design, evaluate, and optimize locally resonant elements for targeted vibration attenuation in an automobile door structure. By utilizing finite-element simulations, this study aims to demonstrate that this targeted multi-frequency configuration can achieve substantial structural displacement reduction with a minimal mass penalty, offering a viable and lightweight alternative to conventional vibration-control solutions.

RESEARCH METHODOLOGIES AND EMPLOYED MATERIALS

To accurately capture localized structural vibrations, the baseline automobile door was modeled as a thin-walled structure with a uniform thickness of 1.2 mm, constructed from standard automotive steel. Simplifications included omitting the window glass, with its mass compensated by applying an equivalent distributed mass along the frame. Numerical simulations were conducted using COMSOL Multiphysics software. The door model was meshed using quadratic tetrahedral elements comprising approximately 125,000 elements, validated through a rigorous mesh-independence study. Rayleigh damping was applied

with a 2% structural damping ratio. The fundamental natural frequencies of the baseline model were preliminarily validated against published experimental modal data for similar automotive panels to ensure computational reliability [27].

A passive vibration suppression method employing locally resonant components was executed to alleviate structural vibrations in the automotive door. Compact resonant elements were incorporated into the door frame and represented as tuned mass-spring subsystems dynamically linked to the host panel. When the stimulation frequency approaches the natural frequency of a resonant element, pronounced local resonance transpires, leading to effective absorption and redistribution of vibrational energy, hence reducing the door's vibration response.

A transmission spectrum analysis of the initial door model was performed to determine the primary vibration frequencies. To evaluate the frequency response objectively, a harmonic point force excitation $F(t) = F_0 sin(2\pi ft)$ with an amplitude F_0 = 10 N was applied normally to the lower surface of the door. The analysis was swept over a frequency interval of 1–200 Hz with a strict frequency increment of 1 Hz. Subsequent to this investigation, three representative target frequencies were identified: 25 Hz, 60 Hz, and 150 Hz.

Resonant elements were developed for each specified frequency utilizing classical vibration theory and band-gap principles. Their geometric and mechanical parameters were parametrically tuned by finite-element simulations in COMSOL Multiphysics to ensure effective local resonance behavior. The elements were systematically arranged into sets and attached to regions exhibiting the greatest displacement. This positioning technique enabled frequency-selective vibration reduction with negligible bulk augmentation and without altering the original door design.

The elastic wave absorption region (band gap) is a specific area within a material or system where the energy of elastic waves, whether sound or mechanical waves, is reduced or eliminated due to the conversion of wave energy into other energy forms (Figure 1). The fundamental theory of acoustic band structures and the design optimization of phononic bandgap materials have been extensively corroborated by classical elastic composite theories [28–30]. This phenomenon occurs when waves pass through materials with varying mechanical or structural properties, leading to wave scattering and gradual energy dissipation [31–33]. To rigorously demonstrate the presence of a true phononic band gap, unit-cell dispersion relations were calculated by applying periodic Bloch-Floquet boundary conditions. The

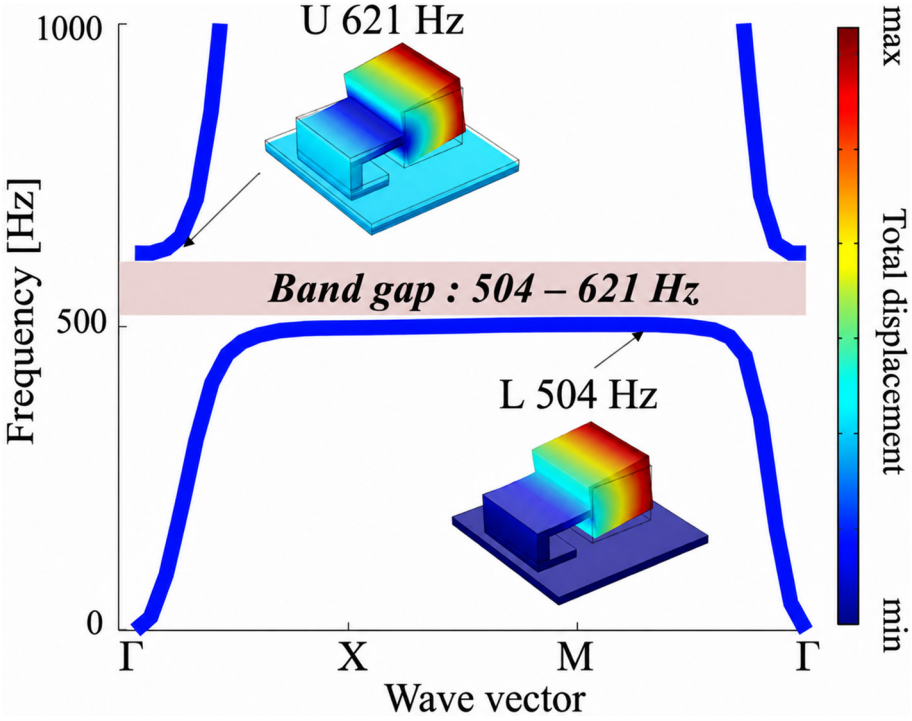


Figure 1. The configuration of the resonant element's elastic wave absorption region

wave-vector path was traced along the contours of the Irreducible Brillouin Zone. The absorption process can reduce the wave's intensity, resulting in its attenuation or complete extinction over time. Regions designated for elastic wave absorption have significant uses in soundproofing, structural engineering, and vibration isolation materials, aimed at improving performance and mitigating the impact of elastic waves in engineering systems.

Research methodology

Wave propagation and irreducible Brillouin zone

In 1946, Brillouin demonstrated that in time-invariant wave systems, the propagation characteristics of waves down an axis are unaffected by the orientation of that axis [34,35]. The irreducible Brillouin zone (IBZ) is defined as a distinct portion of the Brillouin zone (BZ) that can be further minimized if the unit cell possesses inherent symmetry [36]. In square and hexagonal crystal lattices, the irreducible Brillouin zone occupies around 1/8 to 1/12 of the Brillouin zone area due to strong symmetry [37].

Common crystal groups such as P4mm and P6mm are frequently employed to precisely ascertain the IBZ region. Florian Maurin and Claus Claeys [38] simulated several phononic crystal structures to ascertain the band gaps and assess the error when constrained to the irreducible Brillouin zone (IBZ). Table 1 and Figure 2 illustrate the basis vectors and the associated geometry of the crystal groups.

Design principles of the resonant absorber

The resonant absorber element is designed with the goal of optimizing the door's vibration reduction capability, based on the following principles.

The elements are designed to have a resonant frequency that coincides with the desired oscillation frequency of the door. For example, the 25 Hz, 60 Hz, and 150 Hz elements are designed to absorb the corresponding frequency bands, matching the system's oscillation limits and characteristics. Oscillation frequency is one of the important parameters in mechanics. Specifically,

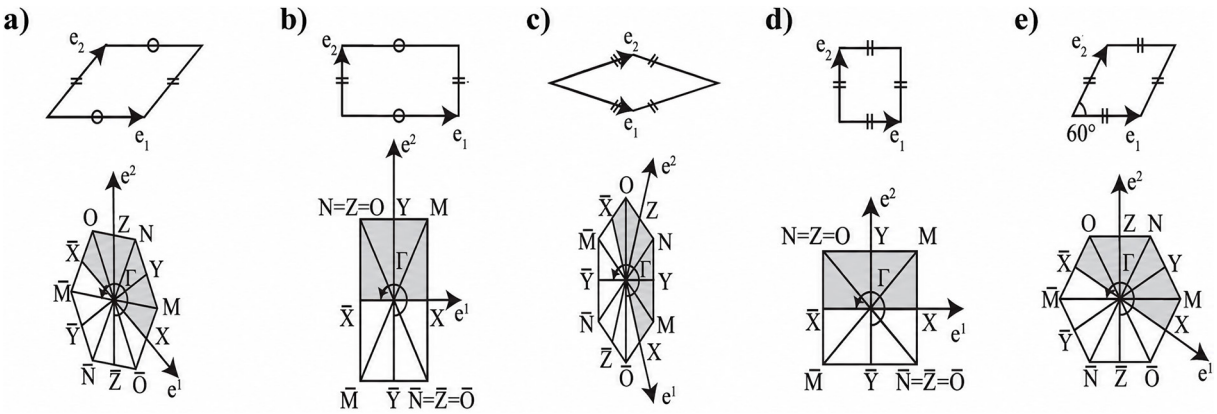


Figure 2. The smallest Brillouin zone has small unit cells

Table 1. Direct and reciprocal basis vectors for five Bravais lattices [38]

Parameter	e_1	e_2	e^1	e^2
Obl.	a(1,0)	b(cosθ, sinθ)	$\frac{1}{a}(1, tan^{-1}\theta)$	$\frac{1}{b}(1, sin^{-1}\theta)$
Rec.	a(1,0)	b(0,1)	$\frac{1}{a}(1,0)$	$\frac{1}{b}(0,1)$
Rho.	a(1,0)	a(cosθ, sinθ)	$\frac{1}{a}(1, -tan^{-1}\theta)$	$\frac{1}{a}(1, sin^{-1}\theta)$
Squ.	a(1,0)	a(0,1)	$\frac{1}{a}(1,0)$	$\frac{1}{a}(0,1)$
Hex.	a(1,0)	$a(\frac{1}{2}, \frac{\sqrt{3}}{2})$	$\frac{1}{a}(1, -\frac{1}{\sqrt{3}})$	$\frac{1}{a}(0, \frac{2}{\sqrt{3}})$

the resonant frequency f0 is often calculated using the formula (Equation 1).

$$f_0 = \frac{1}{2\pi}\sqrt{\frac{k}{m}} \quad (1)$$

where: f_0 is the resonant frequency, k is the equivalent stiffness of the system, m is the effective mass of the system.

a) Design based on band gap regions – these elements are designed to create band gaps within specific frequency ranges, enabling efficient absorption of waves with frequencies within this region. The process of determining the localized displacement region and band gap width is carried out on FEM software (COMSOL), ensuring that the element has good absorption capabilities at the target frequencies.
b) Consolidating several components into a set – rather than installing each component separately, the components are aggregated into sets, facilitating easier adjustment and installation while enhancing vibration absorption efficiency. A configuration of seven resonant elements linked in series optimizes the absorption area and minimizes the system's overall weight.
c) Consolidate the base plates are lightweight and slender – the element's base plates are lightweight and minimally impact the structure, facilitating adjustments in quantity and installation location without substantially increasing overall weight, while preserving vibration reduction efficacy. Crucially, the mechanical connection between the locally resonant elements and the host automobile door was assumed to be perfectly bonded (rigidly tied) in the numerical model, reflecting an ideal high-strength structural adhesive or welding scenario..
d) Explicitly delineate the open and closed states of the element – the element is engineered to modulate the band gap at designated frequencies, facilitating the absorption of waves within the ranges of 24–29 Hz, 55–62 Hz, and 148–159 Hz, aligning with the system's objectives for vibration attenuation.
e) Simulation and optimization evaluation –the simulation procedures in FEM software provide the examination of the band gap region, the influence of the element on displacement, and the absorption capacity, thus enabling the parametric tuning of size, mass, and position to attain maximal reduction efficiency.

EMPLOYED MATERIALS

X3NiCoMoTi 18-9-5 steel is a high-performance alloy steel characterized by its nearly negligible carbon content [39,40]. This steel possesses exceptional tensile strength, elevated hardness, toughness, and favorable machinability and weldability, making it suitable for rigorous applications in aerospace, military, and industrial sectors (Figures 3, 4; Table 2). To address the specific manufacturing process, the elastic modulus (167.5 GPa) selected for the simulations was explicitly chosen to represent the heat-treated condition of additively manufactured (3D-printed) X3NiCoMoTi 18-9-5 steel, as well as to account for fatigue crack growth properties documented in recent literature [41–43]. It is important to emphasize that while metal additive manufacturing is proposed as the fabrication method, no physical specimens were produced in this study. The manufacturability and the corresponding mechanical properties are exclusively numerical assumptions based on experimental data from prior studies.

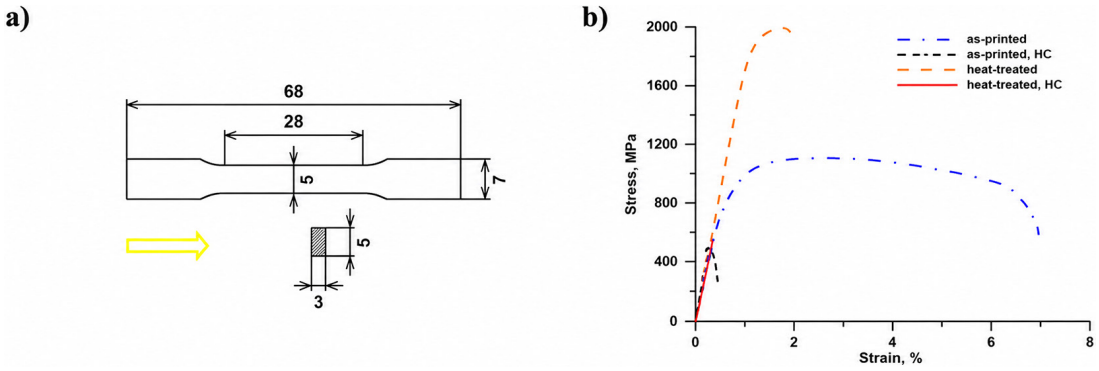


Figure 3. Tensile stress outcomes for X3NiCoMoTi18-905 steel material

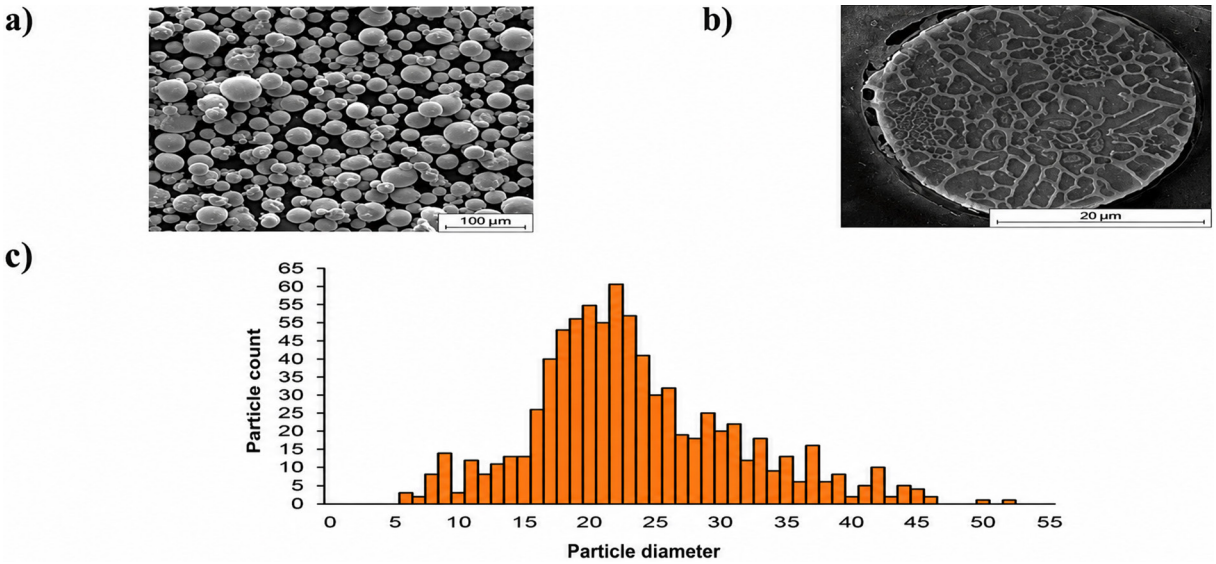


Figure 4. Characteristics of X3NiCoMoTi 18-9-5

A critical parameter in passive vibration control is the mechanical connection between the resonators and the host structure. In this finite-element model, the attachment interfaces (the base plates of the resonators) were modeled as perfectly bonded (rigidly tied) to the door surface. This assumes an ideal connection, equivalent to a high-strength structural adhesive or continuous weld, ensuring complete vibrational energy transmission without interfacial damping or slip.

Alternative model

Alternative computational framework

The equivalent circuit model for the resonant elements and the formula for determining the oscillation frequency of the resonant element will be computed in accordance with the Equation 2. This computer model optimizes design and establishes a robust basis for modifying the parameters of the resonant element to attain maximum efficacy in managing structural waves (Figures 5).

$$f_1 = \frac{1}{2\pi}\sqrt{\frac{k_1}{M_d}}\,;\, f_2 = \frac{1}{2\pi}\sqrt{\frac{k_2}{M_d}} \tag{2}$$

where: f_1 and f_2 are the target natural frequencies of the dual-branch resonant element, k_1 and k_2 represent the equivalent bending stiffness of the corresponding supporting beams, M_d is the concentrated dynamic resonance mass at the end of each beam.

Resonant element model

The baseline metamaterial configurations referenced in similar automotive structural studies

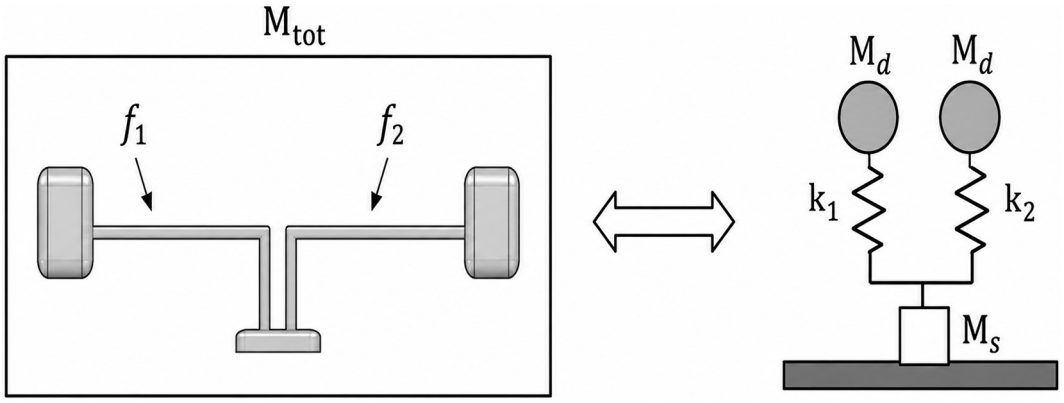


Figure 5. Resonant component (left) and corresponding model (right)

Table 2. Material characteristics of X3NiCoMoTi 18-9-5 steel [44]

Material	Elastic modulus (E)	Density (ρ)	Poisson (ν)
X_3NiCoMoTi 18-9-5 steel	167.5 GPa	8050 kg/m^3	0.3

[44, 45] have a band gap region from 231 Hz to 243 Hz. However, the study's target frequencies are the regions around three target values: 25 Hz, 60 Hz, and 150 Hz. To meet the bandgap requirements in these frequency ranges, three resonant element structures will be designed accordingly. Additionally, the material used for these elements is X3NiCoMoTi 18-9-5 steel, which has superior mechanical properties and meets the technical requirements. A general design model is presented in Figure 6, and the dimensional and volumetric parameters of the elements are listed in Tables 3 and 4.

RESULT AND DISCUSSION

The simulation was conducted on a minimalist model [17] by applying oscillating forces to the door model and concurrently monitoring the lower door displacement in response to excitation frequencies of 25 Hz, 60 Hz, and 150 Hz (Figure 7).

To objectively demonstrate the selection of the characteristic frequencies, a frequency-response function (FRF) covering the entire investigated range of 1 to 200 Hz was extracted prior to the installation of resonators. The outcomes of the door displacement tests within the frequency range of 1 to 200 Hz indicate that at each frequency, the cases of door displacement

Table 3. Geometric specifications of the resonant components

PTCH			
Parameter (mm)	25 Hz	60 Hz	150 Hz
A	8.0	7.0	5.0
B	7.5	7.0	5.0
C	6.0	6.0	5.0
D	6.05	6.05	6.05
E	1.0	1.0	1.0
F	4.6	4.6	4.6
H	14.5	13	10
I	45	39	28
L_1	50	40	30
T	0.6	0.6	0.6
R_1	0.9	1.0	1.1
R_2	1.0	1.1	1.2
R_3	0.2	0.2	0.2
R_4	1.0	1.0	1.0

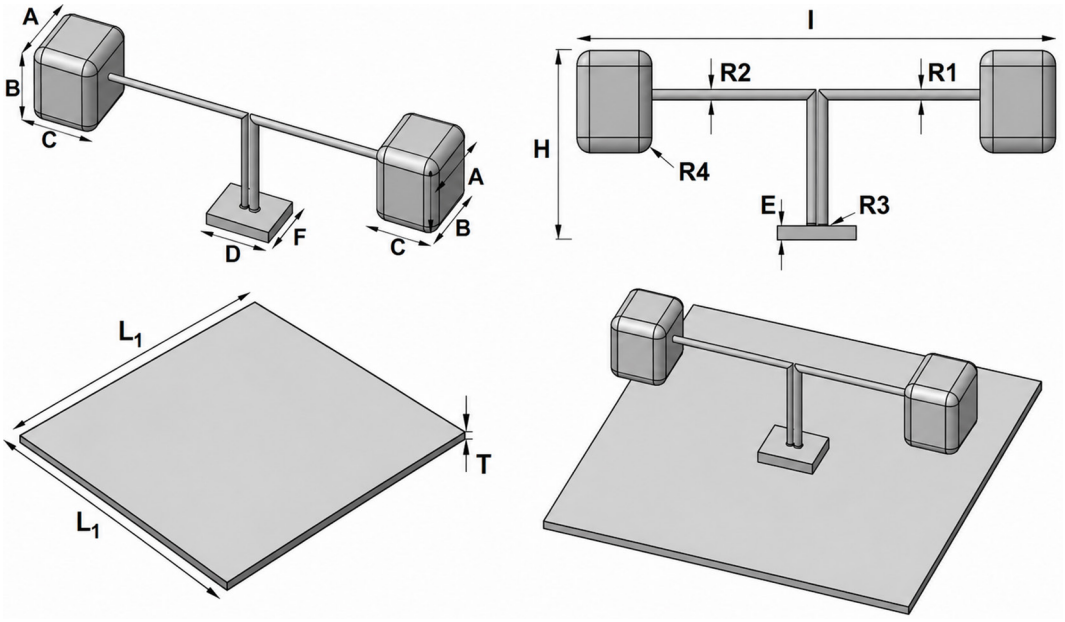


Figure 6. Comprehensive resonant particle model

Table 4. Mass characteristics of the resonant components

PTCH			
Mass (kg)	25 Hz	60 Hz	150 Hz
Resonance mass	6.0 x 10^{-3}	3.0 x 10^{-3}	1.57 x 10^{-3}
Beam	3.0 x 10^{-3}	2.0 x 10^{-3}	1.0 x 10^{-3}
Lining base	2.0 x 10^{-3}	1.36 x 10^{-3}	1.0 x 10^{-3}
Total	11 x 10^{-3}	6.36 x 10^{-3}	3.57 x 10^{-3}

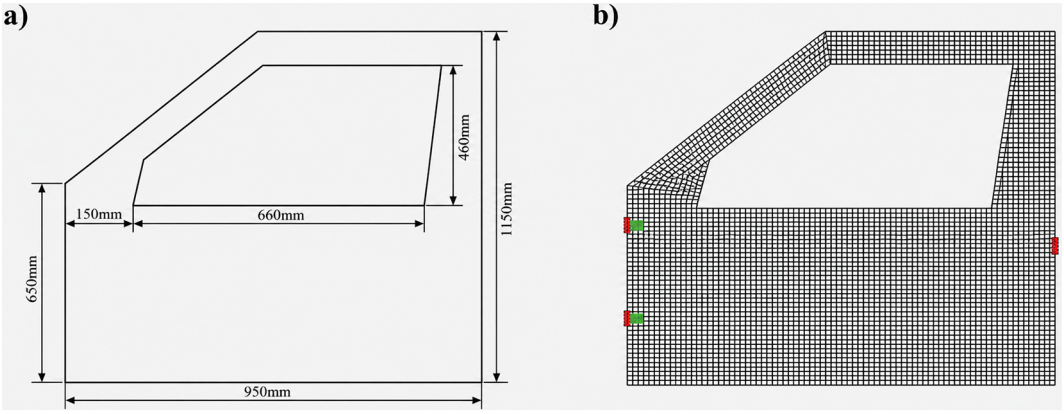


Figure 7. Minimalist door model [17]

predominantly vary in the quantity of displacement zones, and the transmission spectra also exhibit differences. This indicates that the oscillatory dynamics impacting the door are highly intricate, necessitating remediation to mitigate the danger of structural damage to the door. The FRF and the motion spectrum analysis clearly identified three distinct maximum resonance peaks at 25 Hz, 60 Hz, and 150 Hz, as illustrated in the displacement fields in Figure 8.

As the stimulation frequency rises from 1 to 200 Hz, the spectrum density of the door displacement markedly increases. When the door is stimulated at a frequency of 25 Hz (Figure 8a), the two most pronounced displacement regions are localized at the left corner of the door and the contact area between the bottom edge of the door and the glass, as indicated by the purple box. Upon increasing the stimulation frequency to 60 Hz (Figure 8b), the door displays nine locations of significant displacement, shown by red boxes. At a stimulation frequency of 150 Hz (Figure 8c), the quantity of pronounced displacement regions rose to 11, highlighted in yellow. The specific

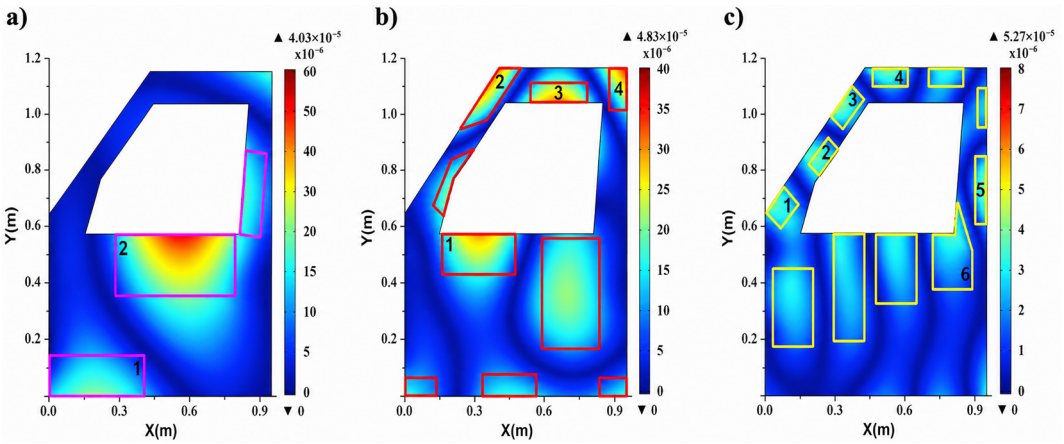


Figure 8. Results of transmission spectrum simulation. a) Door when excited at 25 Hz frequency; b) Door when excited at 60 Hz frequency; c) Door when excited at 150 Hz frequency

parameters for the maximum displacement (D) and the quantity of moving zones of the door are documented in statistical Table 5. Regions exhibiting elevated vibration amplitudes are typically localized near the interface between the door and the glass. Consequently, these regions have been designated and enumerated progressively in Figure 8. These are optimal sites for the installation of resonant components to mitigate vibrations on the car door. This installation site was selected to maximize the high efficiency of utilizing the resonant element's band gap.

The effect of the set of resonant elements attached to the door

To maintain impartiality in assessing the influence of resonant elements on the door, the research methodology will separately simulate each resonant element at frequencies of 25 Hz, 60 Hz, and 150 Hz, therefore elucidating the distinct roles and effects of each element. This facilitates precise determination of the influence of each vibration frequency on the door structure under specific conditions. Moreover, synthetic simulation will provide the examination of interactions among resonant elements during concurrent operation, thereby providing a thorough assessment of the resonant element system's efficacy in enhancing the door's vibration absorption capacity (Figure 9).

Door with a 25 Hz resonant component added

When stimulated at a frequency of 25 Hz, the vibrations attain their maximum intensity and amplitude in two regions (1) and (2) in Figure 10(a). To mitigate these vibrations, it is recommended to install a cluster of four vibration-damping elements in region (2) and six resonant elements in region (1), placed consecutively as depicted in Figure 10 (b). The outcomes and pertinent factors are elaborated upon in Table 6. Following the installation of the resonant parts, the vibration simulation proceeded. The absorbent elements, weighing a total of 0.770 kg, substantially diminished the door's vibration displacement amplitude, reducing it by a factor of 8.84

Table 5. Maximum displacement and quantity of concentrated oscillation zones of the door at frequencies of 25 Hz, 60 Hz, and 150 Hz

Resonance frequency	Displacement (m)	Number of focus zones
25 Hz	4.42×10^{-3}	2
60 Hz	4.04×10^{-3}	9
150 Hz	5.27×10^{-3}	11

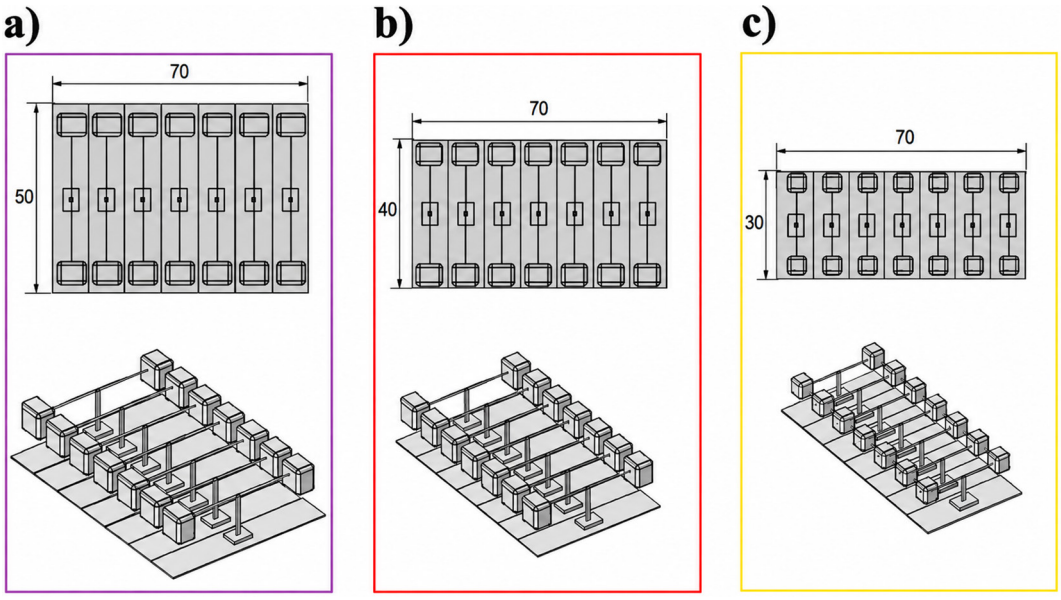


Figure 9. Door-mounted component assembly. a) 25 Hz; b) 60 Hz; c) 150 Hz

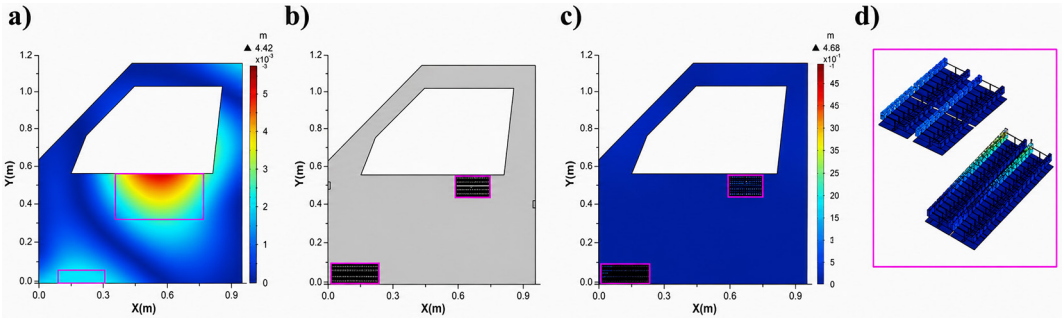


Figure 10. Transmission spectrum of the door and the response of the resonant element under 25 Hz excitation

Table 6. Number and simulation results of doors using 25 Hz resonant parts

Number of element sets	Number of elements	Total mass (kg)	A_{25} (m)	B_{25} (m)	C_{25}
10	70	0.77	4.43×10^{-3}	5×10^{-4}	8.84

from its original state. This outcome illustrates the greater efficacy of the element in absorbing 25 Hz frequencies, hence augmenting vibration reduction capabilities and improving system stability.

The numerical simulations indicate that when the door is equipped with 25 Hz resonant elements, the vibration reduction efficiency attains a significant level, illustrating the exceptional efficacy of these elements in absorbing excitation frequencies. The simulation was subsequently conducted at an excitation frequency of 60 Hz, utilizing resonant elements tuned to 60 Hz for the door. Figure 10 (b) illustrates the four regions exhibiting the most significant displacement; nevertheless, to enhance the efficacy of vibration-absorbing elements, the study recommends the installation of four sets in region (1) and two sets in region (3), as depicted in Figure 8. Given that region (3) is situated between regions (2) and (4), and there exists a strong correlation in vibration, the recommended approach is to initially install in region (3) and subsequently conduct an assessment of the outcomes. The specific specifications for the elements and displacements are documented in Table 4. Noting that the original displacement was $4.04*10^{-3}$ m and, after designating resonant elements, it became $15* 10^{-4}$ m, the performance efficiency diminished by about threefold to a significant degree.

Door with a 60 Hz resonant component added

The numerical simulations indicate that equipping the door with 25 Hz resonant elements significantly enhances vibration reduction efficiency, illustrating the exceptional efficacy of these elements in attenuating excitation frequencies. A simulation was subsequently conducted at an excitation frequency of 60 Hz, utilizing resonant elements tuned to 60 Hz for the door.

Figure 11 illustrates the four regions exhibiting the most significant displacement; nevertheless, to enhance the efficacy of the oscillating absorber elements, the study recommends the installation of four sets in region (1) and two sets in region (3), as depicted in Figure 11. Given that region (3) is situated between regions (2) and (4) and exhibits a strong correlation in vibration, the recommended approach is to initially install in region (3) followed by an assessment of the outcomes. The absorbent elements, weighing a total of 0.267 kg, effectively mitigated the vibrations. Comprehensive parameters for the elements and displacements are documented in table 7. The initial displacement is 4.04×10^{-3} m, and after attaching the resonant elements, it decreased to 1.0×10^{-3} m, meaning the vibration amplitude diminished by a factor of 4.04.

Door with a 150 Hz resonant component added

The simulation processes for the door equipped with resonators at frequencies of 25 Hz and 60 Hz elucidated the precise direction concerning the absorption capacity of the resonant components. We will now conduct the simulation for the door with the resonant element affixed at a frequency of 150 Hz, analogous to the procedures performed at the two preceding frequencies. The location for

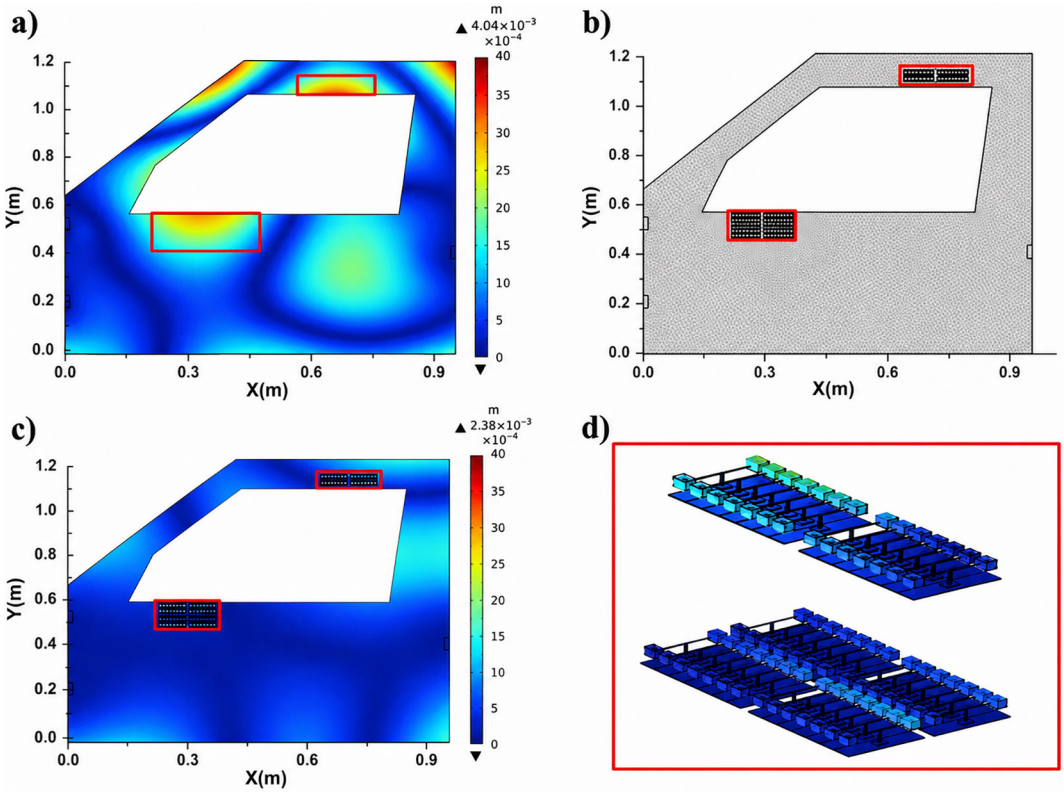


Figure 11. Transmission spectrum of the door and the response of the resonant element under 60 Hz excitation

Table 7. Number and results of door simulations utilizing 60 Hz resonant parts

Number of element sets	Number of elements	Total mass (kg)	A_{60} (m)	B_{60} (m)	C_{60}
6	42	0.267	4.04×10^{-3}	15×10^{-4}	4.04

affixing the resonant element is specified in the indicated regions (1–5) in Figure 8(c). The model, subsequent to the incorporation of this resonant feature, is depicted in Figure 12(b), with the parameters and simulation results elaborated in Table 8.

The findings indicate that with a total mass of 0.175 kg affixed to the door and a resonance frequency of 150 Hz, the efficiency of vibration absorption exceeds fivefold. Consequently, while examining the outcomes for each instance of the door with linked resonant parts, the data presented in Tables 6 to 8 indicates that the minimum displacement reduction ratio is 4.04 times. The incorporation of resonant elements at frequencies of 25 Hz, 60 Hz, and 150 Hz significantly enhanced vibration absorption and diminished door movement at specified frequencies. To confirm and optimize the extensive application of the resonant element, the subsequent phase will involve concurrently simulating the effects of all these element sets on the door.

Examination of door displacement with all resonant components affixed

The installation positions of the component pieces will remain identical to those in the prior simulations, corresponding to the fixed frequencies that were examined. The door attachment model comprises the designated attachment sites for the 25 Hz, 60 Hz, and 150 Hz frequencies illustrated in Figure 13. Figure 14 will present the final displacement findings of the door, offering a clear visual representation of its vibration. Results of the evaluation are presented in Table 9.

The transmission spectrum in Figure 14 and the displacement results in Table 9 indicate a substantial decrease in the structure's vibrational response and total displacement following the installation of the resonant parts. The elements are positioned at sites of significant vibration amplitudes, functioning as energy absorbers and efficiently diminishing vibration in accordance

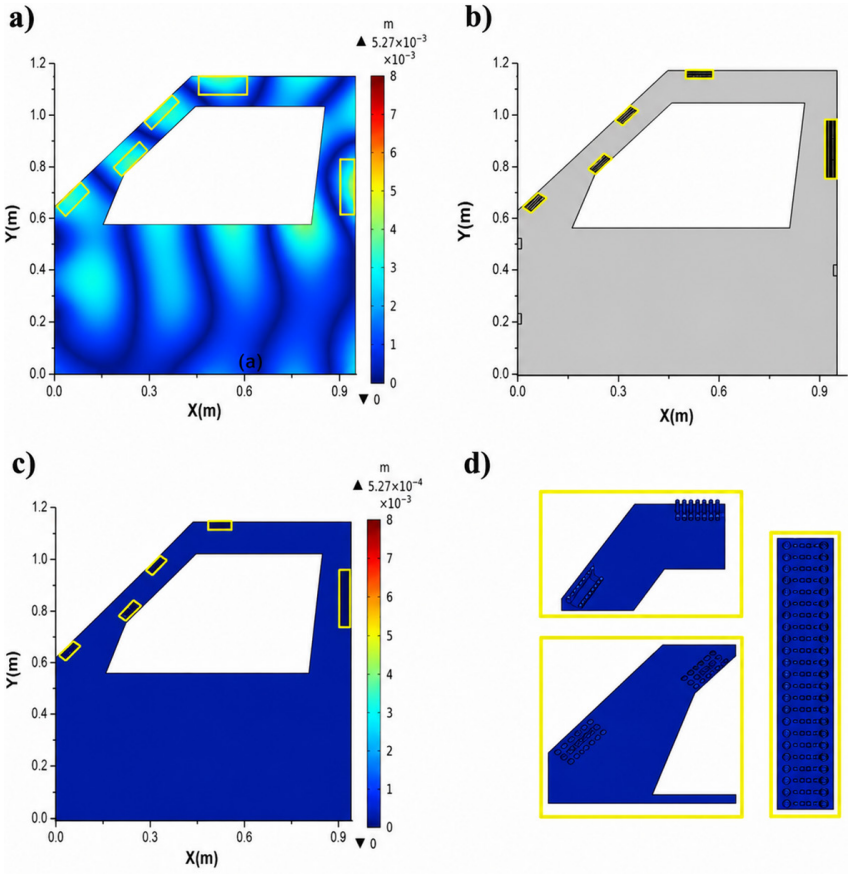


Figure 12. Propagation of the door and the response of the resonant element when stimulated at a frequency of 150 Hz

Table 8. Number and results of door simulations utilizing 150 Hz resonant parts

Number of element sets	Number of elements	Total mass (kg)	A_{150} (m)	B_{150} (m)	C_{150}
7	49	0.175	5.27×10^{-3}	1.0×10^{-3}	5.27

with the theory of spring-mass oscillation. The attenuated vibration amplitudes for frequencies of 25 Hz, 60 Hz, and 150 Hz are 5.0×10^{-4} m, 1.0×10^{-3} m, and 1.0×10^{-3} m, respectively. These significantly lower displacement values help prevent fatigue damage and assist in preserving the structural integrity under deterministic harmonic excitation.

It is critical to evaluate the performance trade-offs, particularly the added mass penalty. The total mass of the combined resonant elements is approximately 1.21 kg, representing only about 7.9% of the baseline structural mass of the simplified door model (15.4 kg). Compared to conventional constrained-layer damping treatments which typically require adding 15% to 25% of the base structure's mass to achieve comparable low-frequency attenuation the proposed locally

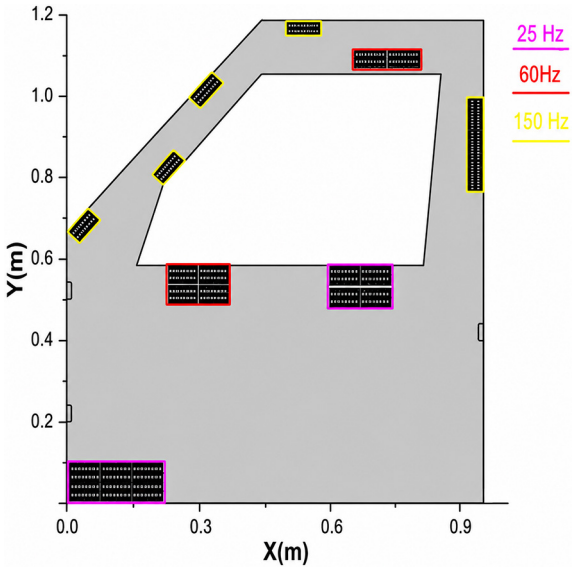


Figure 13. The door model designates resonance frequencies at 25 Hz, 60 Hz, and 150 Hz

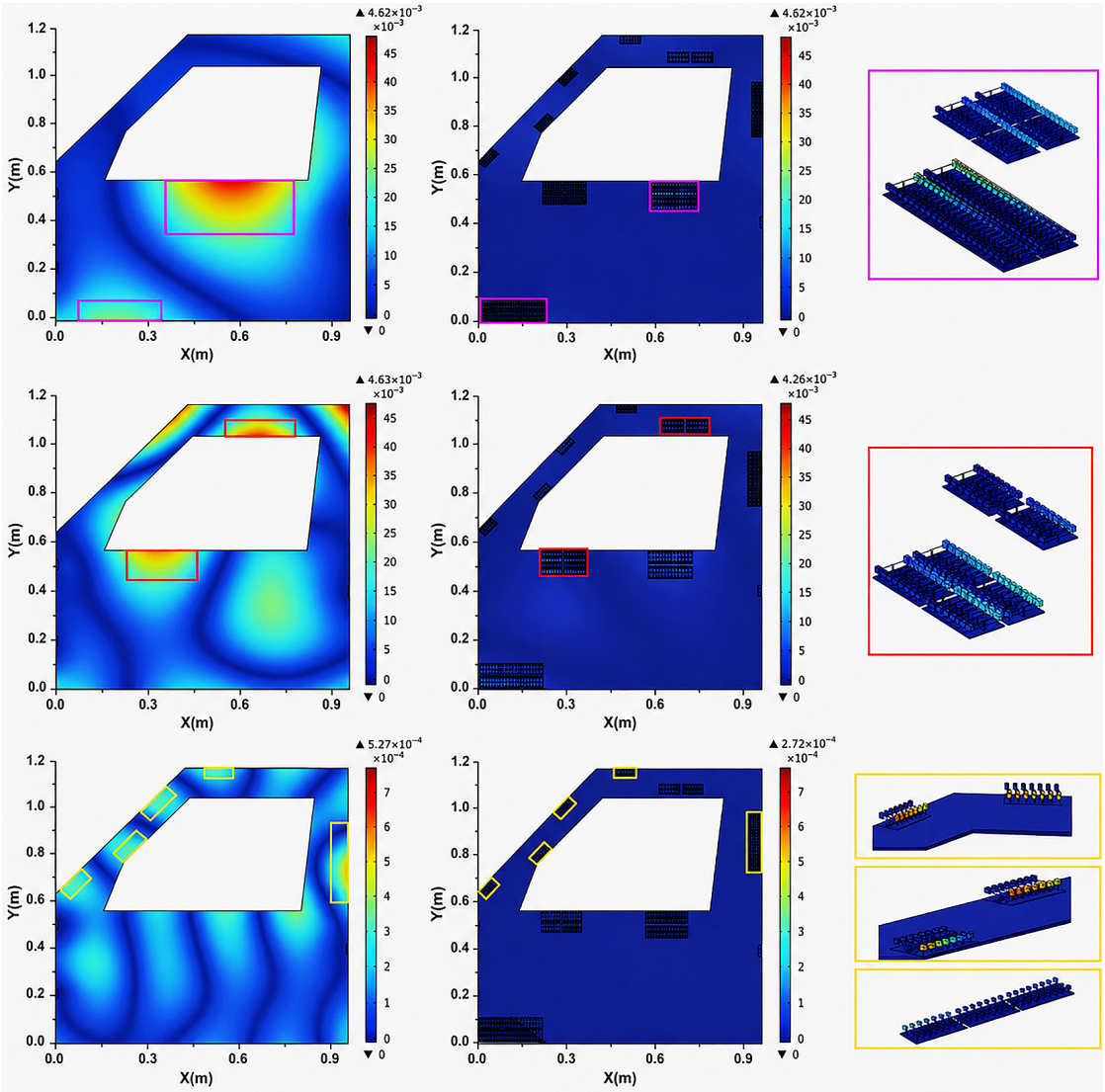


Figure 14. The modal transformation of the door model encompasses all resonant components

Table 9. Results of the transposition on the door with all resonant parts affixed

PTCH	Number of element sets	Mass (kg)	Door displacement without installation (m)	Door displacement with installation	Reduction ratio before and after
25 Hz	10	0.77	4.43×10^{-3}	5.0×10^{-4}	8.84
60 Hz	6	0.267	4.04×10^{-3}	1.0×10^{-3}	4.04
150 Hz	7	0.175	5.27×10^{-3}	1.0×10^{-3}	5.27

resonant setup is significantly more mass-efficient. The differing reduction ratios achieved among the three frequencies are attributed to the varying modal modal participation factors and the localized spatial distribution of the vibration modes on the door surface, which is consistent with findings on multiple structural stop bands in waveguides [46]. However, a limitation to this high-efficiency attenuation is its sensitivity. Locally resonant systems, such as phononic metamaterials and tuned mass absorbers, are highly sensitive to manufacturing tolerances, geometrical deviations, and material damping variations. Any discrepancy in the 3D printing process could shift the target resonance frequency of the elements, potentially detuning the system and reducing its effectiveness. Therefore, an extensive sensitivity and robustness analysis under broadband and stochastic real-vehicle excitation should be performed in future experimental validation phases.

CONCLUSIONS

This study examines the impact of resonant elements on the vibration absorption capacity of door constructions. Utilizing fundamental oscillation theory, the open and closed ranges of absorption regions (bandgap) have been established to enhance the application of resonant elements for the designated object, namely a car door. The numerical findings indicate that resonant devices capable of generating a broad bandgap can achieve significant vibration attenuation efficiency at targeted frequencies of 25, 60, and 150 Hz.

Simulation models indicate that affixing resonant elements to the door does not alter the overall structure's shape due to their diminutive size, while markedly improving vibration absorption capability. The investigation numerically validated the efficacy of locally resonant elements in substantially diminishing multi-frequency vibrations while preserving the structural's geometric integrity.

Despite the promising numerical results, this study has certain limitations. The investigation was exclusively computational and based on a simplified geometric representation of an automobile door. Future research should focus on experimental modal validation using additively manufactured prototypes, evaluating the performance under broadband vehicle excitation, and analyzing the structural robustness against manufacturing tolerances.

Acknowledgments

The authors hereby declare that this research was conducted independently and did not receive any financial support, grant, or funding from any governmental, commercial, or non-profit organization. All analyses, experiments, and interpretations presented in this study were carried out solely by the authors without external influence.

REFERENCES

1. Harikrishnan P.M., Gopi V.P. Vehicle vibration signal processing for road surface monitoring. IEEE Sens. J. 2017; 17(16): 5192–5197. https://doi.org/10.1109/JSEN.2017.2719865
2. Gueta L.B., Sato A. Classifying road surface conditions using vibration signals. In: 2017 Asia-Pacific Signal and Information Processing Association Annual Summit and Conference APSIPA ASC, Kuala Lumpur, Malaysia, Dec 12-15; 2017. https://doi.org/10.1109/APSIPA.2017.8281999
3. Nguyễn T.C. Simulation of internal combustion engine vibration and its effect on the ride comfort of passenger cars (in Vietnamese). Thai Nguyen University; 2009.
4. Gloerfelt X. Noise from automotive components. Arts et Métiers ParisTech, France; 2009.
5. Wang H., Zhang C., Jiang J., Huang W., Guo D., Sheng T. Vibration characteristics and isolation in vibration-sensitive areas under moving vehicle load. Soil Dyn. Earthq. Eng. 2022; 153: 107077. https://doi.org/10.1016/j.soildyn.2021.107077
6. Lu Y., Khajepour A., Soltani A., Li R., Zhen R., Liu Y., Wang M. Gain-adaptive Skyhook-LQR: a coordinated controller for improving truck cabin dynamics. Control Eng. Pract. 2023; 130: 105365. https://doi.org/10.1016/j.conengprac.2022.105365
7. Li J., Zhu X., Zhang C., Dang S., Chen G. CFD simulation of passenger car aerodynamics and body parameter optimization. Fluid Dyn. Mater. Process. 2025; 21(9): 2305–2329. https://doi.org/10.32604/fdmp.2025.067087
8. Trần T.T.H. Simulation of active suspension system vibration considering the influence of hydraulic actuators (in Vietnamese). J. Sci. Technol. Univ. Da Nang. 2022; 20(5).
9. Chen X., Li J., Zhao Y. Multi-directional piezoelectric energy harvesting for vehicle vibration control and condition monitoring. Energy. 2024; 265: 126301.
10. Emond W., Zare M. Can acceleration-coded vibrations help alleviate passenger motion sickness? Investigation in stop-and-go passenger rides. Appl. Ergon. 2026; 132: 104682. https://doi.org/10.1016/j.apergo.2025.104682
11. Nguyễn H.Q. Study on the vibration of assembled trucks in Vietnam when transporting timber on forestry roads (in Vietnamese). Vietnam National University of Forestry; 2018.
12. Bouadi M., Jiang R., Jia B., Yuan K., Zheng S. Dynamics of traffic oscillations in stochastic linear car-following models considering reaction delay: Analytical investigation and numerical analysis. Transp. Res. Part B Methodol. 2026; 211: 103540. https://doi.org/10.1016/j.trb.2026.103540
13. Wu Y., Ma Z., Wang Y., Jiang Y., Yao Z. Nonlinear dynamics of traffic flow stability: A review from car-following to mixed-autonomy. Chaos Solitons Fractals 2026; 208(Part 4): 118340. https://doi.org/10.1016/j.chaos.2026.118340
14. Zheng S.T., Jiang R., Jia B., Tian J., Bouadi M., Makridis M.A., Kouvelas A. A parsimonious enhanced Newell's model for accurate reproduction of driver and traffic dynamics. Transp. Res. Part C Emerg. Technol. 2023; 154: 104276. https://doi.org/10.1016/j.trc.2023.104276

15. Nguyễn Thanh T., Khấu T.P., Nguyễn Hoàng N. Study on the effect of speed on the vibration of Toyota Vios 1.5G when passing speed bumps (in Vietnamese). J. Mar. Sci. Technol. 2021; (Special Issue): 218–222.
16. Nguyễn T.T., Nguyễn T.Q. Development of a vibration experimental model for light truck transmission systems (in Vietnamese). In: Proceedings of the 5th National Conference on Mechanical Engineering (VCME 2018), Hanoi, Vietnam, Oct; 2018.
17. Zhang S., He Z.C., Xiao X. Design and application of laminate acoustic metamaterials for low-frequency structural vibration suppression. Composite Structures. 2024; 305: 116514.
18. Bachy E., Jaboviste K., et al. Investigations on the performance and robustness of a metasorber designed for structural vibration mitigation. Mech. Syst. Signal Process. 2022; 170: 108830. https://doi.org/10.1016/j.ymssp.2022.108830
19. Lin B., Huang W., Wang Z., Si K., Zhou X., Xu F. Design and analysis of an ultra-thin metamaterial absorber for C, X, Ku and K band applications. Mater. Today Phys. 2026; 60: 102008. https://doi.org/10.1016/j.mtphys.2025.102008
20. Guo L., Zhao S., Guo Z., Zhang Y., Yang J., Kitipornchai S. Phase transition-based tunable phononic crystals and metamaterials: A review. Thin-Walled Struct. 2026; 218(Part A): 113984. https://doi.org/10.1016/j.tws.2025.113984
21. Sangiuliano L., Claeys C., Deckers E., De Smet J., Pluymers B., Desmet W. Locally resonant metamaterial patches on rear shock towers of a vehicle to reduce structure-borne road noise: Numerical and experimental performance validation. In: Automotive Acoustics Conference 2019. Springer; 2020. https://doi.org/10.1007/978-3-658-27669-0_10
22. Rocha de Melo Filho N.G. Optimisation based design of a metamaterial foam core sandwich panel with in-core resonators. In: Proceedings of Inter-Noise 2020, Seoul, Republic of Korea; 2020.
23. Yu J., Nerse C., Chang K.J., Wang S. A framework of flexible locally resonant metamaterials for attachment to curved structures. Int. J. Mech. Sci. 2021; 204: 106533. https://doi.org/10.1016/j.ijmecsci.2021.106533
24. Liao Y., Huang H., Chang G., Luo D., Xu C., Wu Y., Tang J. Research on low-frequency noise control of automobiles based on acoustic metamaterial. Materials (Basel). 2022; 15(9): 3261. https://doi.org/10.3390/ma15093261
25. Wu X., Sun L., Zuo S., Liu P., Huang H. Vibration reduction of car body based on 2D dual-base locally resonant phononic crystal. Appl. Acoust. 2019; 151: 1–9. https://doi.org/10.1016/j.apacoust.2019.02.020
26. Xin Y.J., Cai P.C., Li P., Qun Y., Sun Y.T., Qian D., Cheng S.L., Zhao Q.X. Comprehensive analysis of band gap of phononic crystal structure and objective optimization based on genetic algorithm. Phys. B Condens. Matter 2023; 667: 415157. https://doi.org/10.1016/j.physb.2023.415157
27. B. B. Kumar, B. T. Chandru, and B. H. Maruthi, Numerical and Experimental Vibration Analysis of Car Door With and Without Viscoelastic Damper. Materials Today: Proceedings. vol. 5, no. 11, pp. 25057–25063, 2018.
28. Abdurakhmonov S., Skvortsov A., Nikolaev V., Ehsan M.A., Din S.U., Ashurov M. Coexisting dual phononic and photonic band gaps in inverse opal phoxonic crystals. Phys. Lett. A 2026; 568: 131225. https://doi.org/10.1016/j.physleta.2025.131225
29. Zhao J., Faruque M.R.I. Low-frequency vibration attenuation using locally resonant acoustic metamaterials in automotive panels. Mechanical Systems and Signal Processing. 2024; 208: 111012.
30. Kushwaha M.S. Classical band structure of periodic elastic composites. Int. J. Mod. Phys. B. 1996; 10(9): 977–1094. https://doi.org/10.1142/S0217979296000398
31. Kushwaha M.S., Halevi P., Martínez G., Dobrzynski L., Djafari-Rouhani B. Theory of acoustic band structure of periodic elastic composites. Phys. Rev. B Condens. Matter. 1994; 49(4): 2313–2322. https://doi.org/10.1103/PhysRevB.49.2313
32. Kushwaha M.S., Djafari-Rouhani B. Complete acoustic stop bands for cubic arrays of spherical liquid balloons. J. Appl. Phys. 1996; 80(6): 3191–3196. https://doi.org/10.1063/1.363245
33. Pennec Y., Djafari-Rouhani B., Akjouj A., Lévêque G., El Boudouti E.H., Al-Wahsh H., Dobrzynski L. Chapter 5 - Transmission in 2D phononic crystals and acoustic metamaterials. Phononics 2018; 271–373. https://doi.org/10.1016/B978-0-12-809948-3.00005-3
34. Born M. Wave propagation in periodic structures. Nature. 1946; 158(4019): 926. https://doi.org/10.1038/158926a0
35. Kittel C. Introduction to solid state physics. 8th ed. John Wiley & Sons; 2005.
36. Cracknell A.P. Tables of the irreducible representations of the 17 two-dimensional space groups and their relevance to quantum mechanical eigenstates for surfaces and thin films. Thin Solid Films. 1974; 21(1): 107–127. https://doi.org/10.1016/0040-6090(74)90095-9
37. Shmueli U., editor. International tables for crystallography. Vol. B, Reciprocal space. 3rd ed. Kluwer Academic Publishers; 2001.
38. Maurin F., Claeys C., Deckers E., Desmet W. Probability that a band-gap extremum is located on the irreducible Brillouin-zone contour for the 17

different plane crystallographic lattices. Int. J. Solids Struct. 2018; 135: 26–36. https://doi.org/10.1016/j.ijsolstr.2017.11.006

39. Sigalas M.M., Economou E.N. Elastic and acoustic wave band structure. J. Sound Vib. 1992; 158(2): 377–382. https://doi.org/10.1016/0022-460X(92)90059-7
40. Strakosova A., Roudnická M., Ekrt O., Vojtěch D., Michalcová A. Hydrogen embrittlement of the additively manufactured high-strength X3NiCoMoTi 18-9-5 maraging steel. Materials (Basel). 2021; 14(17): 5073. https://doi.org/10.3390/ma14175073
41. Strakosova A., Kubásek J., Michalcová A., Průša F., Vojtěch D., Dvorský D. High strength X3NiCoMoTi 18-9-5 maraging steel prepared by selective laser melting from atomized powder. Materials (Basel). 2019; 12(24): 4174. https://doi.org/10.3390/ma12244174
42. Gong J., Xiao X., Ai C., Yin Y., Wang H., Song Z., Wu Z., Yang Z., Li H., Yu H. A critical review on mechanical properties regulation strategies of laser additive manufacturing (LAM) metal components: Process optimization, composition and structural design. J. Mater. Res. Technol. 2026; 43: 2421–2462. https://doi.org/10.1016/j.jmrt.2026.06.221
43. Suryawanshi J., Prashanth K.G., Ramamurty U. Tensile, fracture, and fatigue crack growth properties of a 3D printed maraging steel through selective laser melting. J. Alloys Compd. 2017; 725: 355–364. https://doi.org/10.1016/j.jallcom.2017.07.177
44. Sangiuliano L., Claeys C., Deckers E., De Smet J., Pluymers B., Desmet W. Low-frequency tyre noise mitigation in a vehicle using metal 3D printed resonant metamaterials. Mech. Syst. Signal Process. 2022; 179: 109335. https://doi.org/10.1016/j.ymssp.2022.109335
45. Sangiuliano L., Claeys C., Van Belle L., Deckers E., Desmet W. Locally resonant metamaterial patches on rear shock towers of a vehicle to reduce structure-borne road noise: Numerical and experimental performance validation. In: Proceedings of the International Conference on Noise and Vibration Engineering (ISMA), Leuven, Belgium; 2018.
46. Claeys C., Rocha de Melo Filho N.G., Van Belle L., Deckers E., Desmet W. Design and validation of metamaterials for multiple structural stop bands in waveguides. Extreme Mech. Lett. 2017; 12: 7–22. https://doi.org/10.1016/j.eml.2016.08.005